Journal of Soft Computing in Civil Engineering 7-4 (2023) 1-23

Contents lists available at SCCE

Journal of Soft Computing in Civil Engineering

Journal homepage: www.jsoftcivil.com

Intelligent Prediction of Unconfined Compressive Strength and Young's Modulus of Lean Clay Stabilized with Iron Ore Mine Tailings and Hydrated Lime Using Gaussian Process Regression

Ali Reza Ghanizadeh[1*], Seyed Saber Naseralavi[2]

1. Associate Professor, Department of Civil Engineering, Sirjan University of Technology, Sirjan, Iran
2. Assistant Professor, Department of Civil Engineering, Shahid Bahonar University of Kerman, Kerman, Iran
Corresponding author: *ghanizadeh@sirjantech.ac.ir*

https://doi.org/10.22115/SCCE.2023.370814.1573

ARTICLE INFO

Article history:
Received: 20 November 2022
Revised: 05 February 2023
Accepted: 04 April 2023

Keywords:
Lean clay stabilization;
Iron ore mine tailing;
Hydrated lime;
Unconfined compressive strength;
Young's modulus;
Gaussian process regression.

ABSTRACT

Chemical stabilization is used to enhance and increase the strength characteristics of soft and problematic soils. In this research, Gaussian Process Regression (GPR) is employed to estimate the unconfined compressive strength (UCS) and the Young's modulus (E) of lean clay soils stabilized with iron ore mine tailing (IOMT) and hydrated lime (HL) percentage. In this regard, four inputs including the moisture content (MC), IMOT percentage, HL percentage, and curing time (CT) were used. The value of R^2 for estimating the UCS and the E were 0.9825 and 0.9633 for all data, respectively. The RMSE for predicting the UCS and the E were 0.1875 and 19.868 for all data, respectively. The result of the sensitivity analysis demonstrated that MC, CT, HL, and IOMT percentage have the highest contribution to the UCS of the stabilized lean clay, respectively. Also, MC, HL, IOMT percentage, and CT have the highest impact on the E of the stabilized lean clay, respectively. The parametric study also revealed that increasing the HL content and the curing time led to an increase in the UCS and the E of stabilized lean clay, while IOMT content and the moisture content has an inverse relationship with the UCS and the E of stabilized lean clay soils.

How to cite this article: Ghanizadeh AR, Naseralavi SS. Intelligent prediction of unconfined compressive strength and Young's modulus of lean clay stabilized with iron ore mine tailings and hydrated lime using gaussian process regression. J Soft Comput Civ Eng 2023;7(4):1–23. https://doi.org/10.22115/scce.2023.370814.1573

2588-2872/ © 2023 The Authors. Published by Pouyan Press.
This is an open access article under the CC BY license (http://creativecommons.org/licenses/by/4.0/).

1. Introduction

In recent years, the need for the construction of various transportation infrastructures, including roads, airports, and railways, has been increasing. A large surface of the subsoil in many construction projects is made of clay, which is not suitable for road construction [1]. Soil stabilization is an approach to improve different characteristics of soils and produce a better construction material [2]. Various additives including but not limited to lime and cement are usually used to stabilize the weak and problematic soils [3]. Mixing these additives with soil improves soil properties, soil strength, permeability, and soil deformation characteristics [4]. Many studies in the past have been conducted to use stabilizing agents in various projects around the world [5,6]. Stabilization of clay soils with lime includes mixing lime with clay and then compacting it at the optimum moisture content (OMC). The lime used to stabilize fine-grained soils is usually in the form of burned limestone products such as quicklime or dolomitic quicklime. In lime stabilization of soil, part of the pozzolanic material is provided by the soil and there is no need for other pozzolanic materials like cement [7]. The investigations conducted on clay soil stabilized with lime show the improvement of soil engineering characteristics such as Atterberg limits, California bearing ratio (CBR), unconfined compressive strength (UCS), and Young's modulus (E) of soil [8–10].

The expansion of mining activities continuously causes an increase in mine tailings, both the tailings resulting from excavation to reach the mineral materials and also the tailings resulting from the processing of mineral materials. The lack of proper management and the accumulation of these wastes around the mines, not only occupy a lot of space, but also lead to negative environmental effects. Reuse of these wastes in large volume is one of the most sustainable ways to solve this problem [11]. Stabilization by IOMT is one of the low-cost and simple solutions to deal with these problems. So that the reuse and recycling of IOMT for civil projects and road construction causes the consumption of tailings and prevents the dangers caused by the pollution of mineral wastes [12]. To date, few research has been done on the technical feasibility of using IOMT for soil improvement in civil engineering and especially road construction materials [12–17]. The results of these studies show that the IOMT stabilized with additives such as lime can be used as road materials [12].

With increasing computing power of computers, several researchers have used soft computing and machine learning methods to develop predictive models for civil engineering problems [18–27]. The feasibility of artificial neural network (ANN) and regression analysis were investigated by Sathyapriya et al. [28] to estimate the UCS of clay soil stabilized with industrial waste. Based on the analysis, both methods have the ability to approximate the UCS based on the soil properties with high precision, but the ANN provided a more accurate estimation. Chore et al. [29] presented different predictive models based on multiple linear regression and ANN to estimate the Brazilian tensile strength and the UCS of soil stabilized with cement, polypropylene fibers, and fly ash. The input parameters included cement percentage, fibers percentage, OMC, and dry density, while the output variables were considered as indirect tensile strength and UCS. The findings of the research revealed the superiority of the accuracy of the ANN for the assessing of compressive and tensile strength. Sihag et al. [30] investigated the application of

decision trees (M5P), group method of data handling (GMDH), and multivariate adaptive regression splines (MARS) to assess the UCS of clay stabilized with ground granulated blast furnace slag, fly ash, and cement. Ghanizadeh et al. [22] used GMDH to evaluate the UCS of clay subgrade stabilized with cement and lime. The findings revealed that the GMDH method can assess the UCS of stabilized clay with high accuracy. Tabarsa et al. [31] utilized ANN and SVM models to assess the UCS of soils stabilized with rice husk ash, cement, and lime. The findings demonstrated the better performance of SVM compared to ANN in assessing the strength of the stabilized soils. Principal component analysis (PCA) and Bayesian model averaging methods were utilized by Do et al. [32] to assess the flexural strength and the UCS of cement-stabilized sandy soils. Pham et al. [33] developed Adaboost models to classify soil type. They used laboratory data to design and validate the new models. Moreover, two models based on ANN and tree models were implemented for the comparison. The results revealed that the Adaboost models exhibited better performance. Tran [34] developed hybrid Gradient Boosting (GB) with different metaheuristic algorithms for predicting the UCS of stabilized soils. The findings indicated the better performance of the hybrid GB model. Armaghani et al. [35] used ANN optimized by genetic algorithm (GA) and PSO to predict soil shear strength of sandy-soil mixed with fibers. It was found that the GA-ANN performed better than the PSO-ANN to estimate soil shear strength. Ghanizadeh et al. [24] used the Evolutionary Polynomial Regression (EPR) method to model the Young's modulus and the UCS of clay soil stabilized with cement and lime. This research showed that the EPR method has the ability to estimate the resistance parameters of stabilized soil. Momeni et al. [36] unitized a hybrid ANN with Gravitational Search Algorithm (GSA) and PSO to investigate the deformation of geogrid reinforced soil (GRS) retaining structures. In this regard, ABAQUS was utilized to simulate a case study for dataset construction. It is discovered that GSA-ANN exhibited better performance than the PSO-ANN. Momeni et al. [37] developed a predictive model based on extreme gradient boosting and slap swarm algorithm to assess the performance of GRS retaining structures. The findings exhibited the feasibility of the hybrid model to predict the performance of GRS retaining structures.

Although extensive research has been done to estimate different properties of various stabilized soil, no model has been presented to the best of author's knowledge so far for estimating of the Young's modulus and the UCS of lean clay stabilized with IOMT and hydrated lime (HL) by means of computational intelligence methods. Recently, GPR method has been successfully applied for regression problems [21,26,38,39] because of the flexibility of their representation and providing uncertainty measures for the predictions [40]. The main objective of this study is to provide a model to assess the E and the UCS of lean clay stabilized with IOMT and HL using Gaussian Regression Process (GPR). In this regard, four inputs including IOMT, HL, MC, and CT were used, while the UCS and the E were considered as the outputs. Furthermore, the sensitivity analysis and parametric analysis have been used in this research to demonstrate the importance of each independent variables and the impact of these variables on the E and UCS of clay stabilized with IOMT and hydrated lime. General research methodology and modeling procedure have been depicted in Fig. 1.

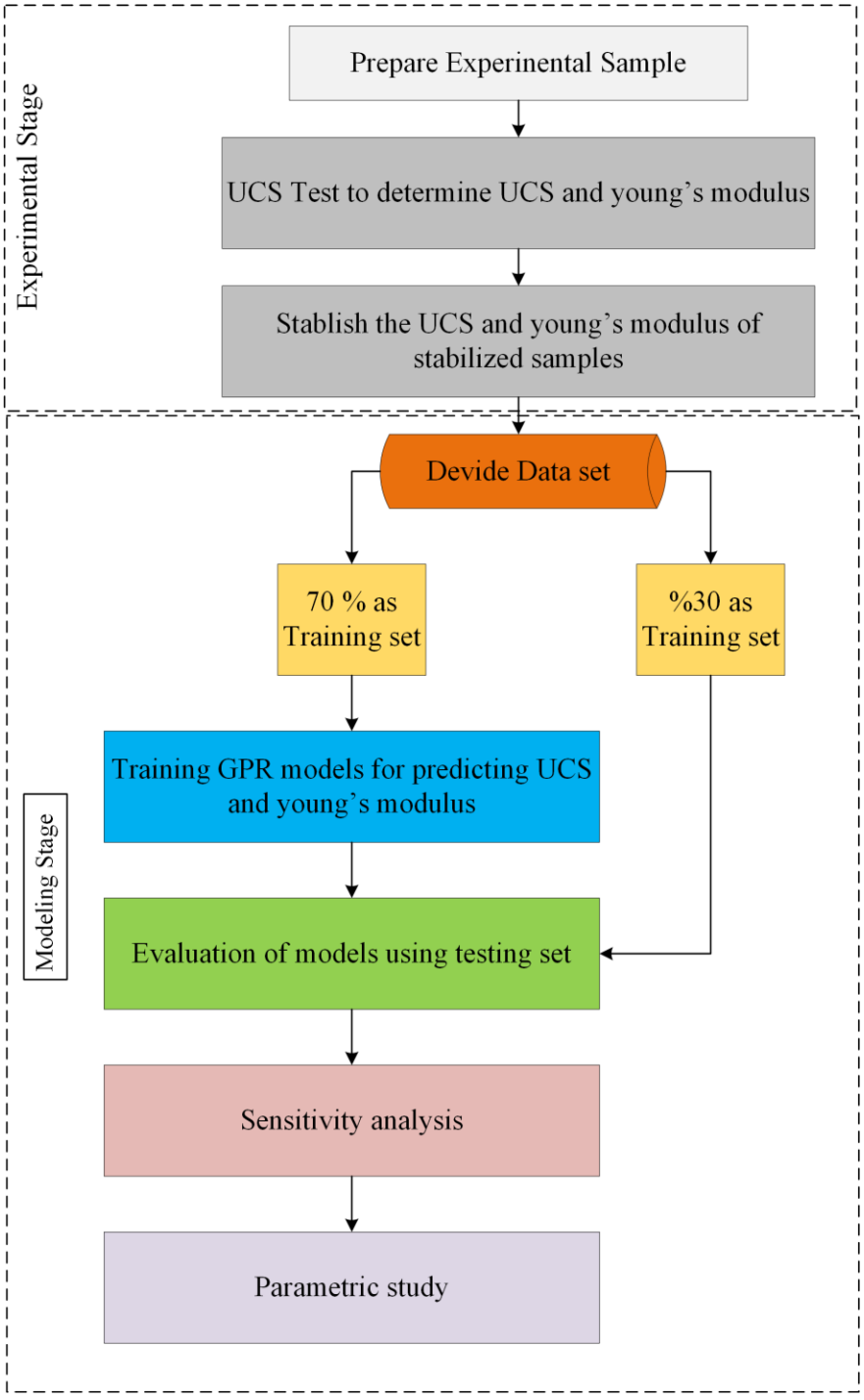

Fig. 1. General research methodology and modeling procedure in this study.

2. Dataset preparation

2.1. Experimental study

The soil used in this research was a lean clay soil collected from a place near city of Sirjan, Iran. Moreover, the IOMT of Golgohar mine in Sirjan were used to prepare the samples. The physical

properties and chemical compositions of lean clay and IOMT are presented in Table 1 and 2, respectively. Moreover, the grain size diagram of the lean clay and the IOMT are depicted in Fig. 2.

Table 1
The properties of lean clay and IOMT.

Properties	Standard	Clay Soil	IOMT
AASHTO Classification	ASTM D3282	A-6	A-2-4
Unified Classification	ASTM D2487	CL	SM
gravity of soil (G_s)	ASTM D854	2.45	2.95
plastic limit	ASTM D4318	22.24	NP
Liquid Limit	ASTM D4318	36.58	NP
shrinkage limit	ASTM D427	17.76	30.43
plasticity index	ASTM D4318	14.34	NP
pH	ASTM D4972	7.7	8.81

Table 2
The chemical compositions of lean clay and IOMT in percent.

Composition	Clay Soil	IOMT
SiO_2	49.482	35.952
Al_2O_3	12.377	5.907
Fe_2O_3	7.592	22.174
CaO	9.099	9.249
Na_2O	0.493	0.937
MgO	4.558	14.158
K_2O	2.856	1.855
TiO2	0.643	0.629
MnO	0.098	0.077
P_2O_5	0.093	0.451
LoI	12.5	1.8

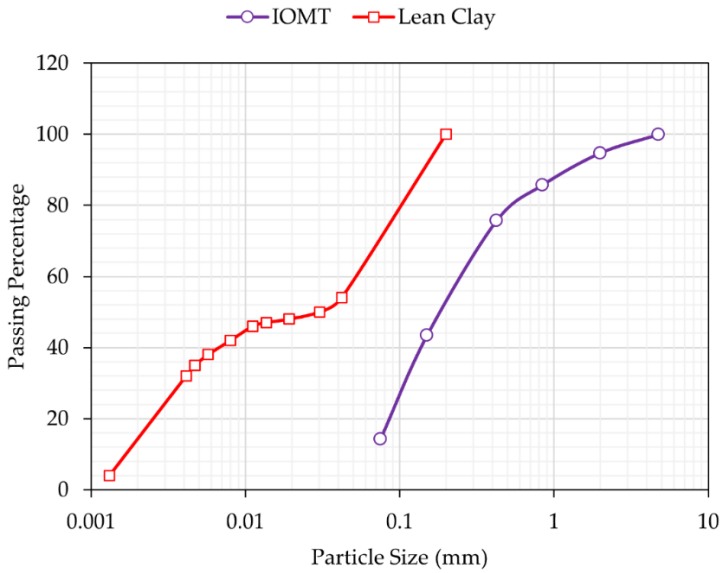

Fig. 2. The particle size of the IOMT and the clay.

The lime within this research was hydrated lime (HL), which conformed to ASTM C977 standards. The chemical compositions of HL are given in Tables 3.

Table 3
The chemical compositions of the hydrated lime (HL).

Compositions	%
$Ca(OH)_2$	90
CaO (Free)	1.5
MgO	1
SiO_2	0.6
AL_2O_3	0.5
Fe_2O_3	0.2
SrO	1.6
LoI	4.6

In this study, different percentages of IOMT (0%, 10%, 20%, and 30%) were combined with the lean clay soil, and then each of the mixed soil samples were stabilized with four percentages of HL (0%, 2%, 4%, and 6%). The standard proctor compaction test was conducted according to ASTM D698 standard to determine the MDD and OMC for each combination. The compaction test on each mixture was done by five-point method (five different moisture percentages) and the MDD and OMC for each mixture were determined. In total, 24 proctor tests were performed to find the MDD and OMC of different mixtures. The results of the compaction test show that by increasing the percentage of iron ore mine tailings in different percentages of HL, the OMC decreases and the MDD increases. The variations of OMC for lime-stabilized samples are recorded from 11.88% to 20.02%, while the MDD varies from 1.72 g/cm^3 to 1.92 g/cm^3.

Based on ASTM D2166, the UCS tests were performed on the several stabilized samples with different iron ore mine tailings contents (0%, 10%, 20%, and 30%) and HL contents (0%, 2%, 4%, and 6%) and compaction moisture content (OMC, 10% more than OMC (wet side) and 10% less than OMC (dry side)) at different curing periods (7, 28, and 56 days). In total, 144 samples with a height of 100 mm and a diameter of 50 mm were made for the UCS test. The samples were placed under the unconfined compressive strength device and loaded at a speed of 1 mm/min to determine the UCS. In addition, the Young's modulus was determined using the slope of the stress and strain diagram obtained from the UCS test results. The whole dataset is reported in the Appendix.

2.2. Statistical description

The dataset used in this study includes 144 samples of four inputs and two outputs. The input variables are IMOT percentage, HL percentage, curing time (CT), and MC, while the output variables are UCS and Young's modulus (E). 70% of the data (101 records) in this research were randomly used for training and 30% of remaining data (43 records) were used for testing. Table 4 shows the statistical descriptions of the data, including the maximum, minimum, mean, median, percentiles and standard deviation (STD) of each input variable for the training set, the testing set, and the total data.

Table 4
Descriptive Statistics of experimental dataset.

	IOMT (%)	HL (%)	MC (%)	CT (Days)	UCS	E
Min	0.00 (0.00) [0.00]	0.00 (0.00) [0.00]	11.88 (11.88) [11.88]	7 (7) [7]	0.59 (0.8) [0.5]	11.34 (7.47) [17.19]
25th Percentiles	0.00 (10.00) [5.00]	0.00 (2.00) [1.00]	14.12 (14.81) [14.22]	7 (7) [7]	1.34 (1.2) [1.3]	79.40 (84.79) [74.14]
Median	20.00 (10.00) [15.00]	2.00 (4.00) [3.00]	15.48 (15.81) [15.61]	28 (28) [28]	2.03 (2.0) [2.0]	144.12 (167.36) [152.37]
Mean	15.35 (14.19) [15.00]	2.85 (3.35) [3.00]	15.55 (15.89) [15.65]	31.33 (28.00) [30.33]	2.44 (2.4) [2.4]	165.74 (173.62) [167.79]
75th Percentiles	30.00 (20.00) [25.00]	4.00 (6.00) [5.00]	16.99 (17.13) [17.06]	56 (56) [56]	3.31 (3.2) [3.1]	238.46 (257.75) [238.42]
Max	30.00 (30.00) [30.00]	6.00 (6.00) [6.00]	20.02 (19.33) [20.02]	56 (56) [56]	6.40 (5.8) [6.5]	418.93 (399.39) [415.62]
STD	11.71 (10.06) [11.22]	2.27 (2.17) [2.24]	1.91 (1.78) [1.87]	20.30 (19.80) [20.14]	1.38 (1.3) [1.4]	103.49 (101.72) [103.97]

1- IOMT, HL, MC, CT, E, and UCS represent the iron ore mine tailing, hydrated lime, moisture content, curing time, Young's modulus, and unconfined compressive strength, respectively.
2- The free numbers, the numbers in the parentheses and the numbers in the brackets represent the values corresponding to the training data, testing data and total data, respectively.

The correlation coefficient between the UCS and the input variables is depicted in Fig. 3(a). As shown, HL and CT demonstrate relatively high correlations with the measured UCS, whereas the IOMT and the MC is weakly correlated with the UCS. Moreover, the correlation coefficient between the E and the inputs is shown in Fig. 3(b). It is observed that HL and CT show relatively high correlations with the measured E, whereas the IOMT and the MC are weakly correlated with the E.

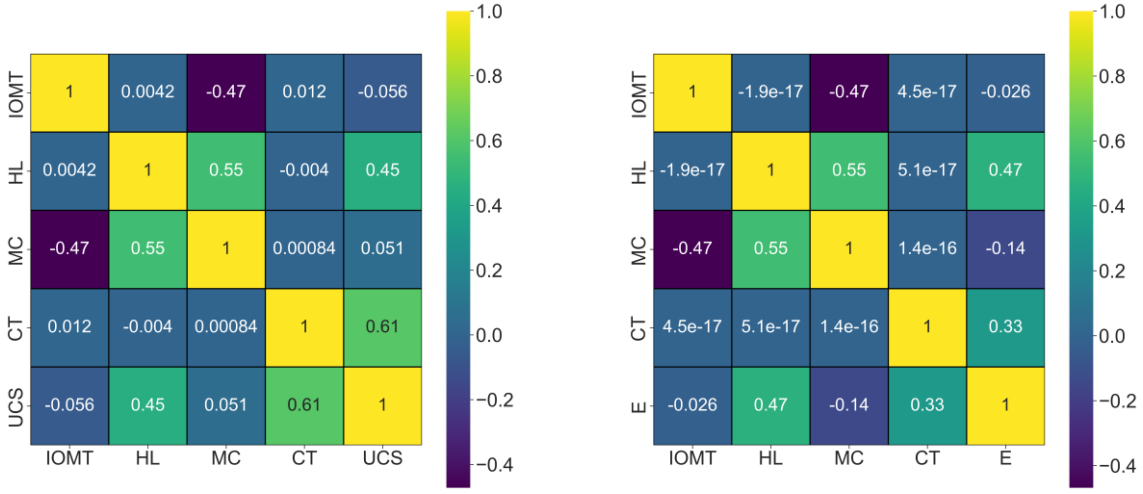

(a) (b)

Fig. 3. Pearson correlation coefficients between variables, (a) UCS and (b) E.

3. Methods

3.1. Gaussian process regression (GPR)

GPR is considered as a non-parametric learning method for probabilistic classification and regression problems. GPR can find complex relationships between inputs and outputs due to the usage of kernel functions. GPR models have been widely used for regression and classification problems in various scientific and engineering problems [21,26,38,41].

Assume $x_i \in \mathbb{R}^d$ is the input data and $y_i \in \mathbb{R}$ is the output data in the training set $S = \{(x_i, y_i)|i = 1, \ldots, n\}$. The main assumption of GPR is presented by Eq. (1):

$$y = f(x) + \varepsilon \tag{1}$$

Where $f(.)$ is an anonymous function, $\varepsilon \sim N(0, {\sigma_n}^2)$ represents the equal noise variance for the input data (x_i), and σ_n denotes the standard deviation of the Gaussian noise. The symbol ~ denotes *sampling for* in statistics.

In the GPR model, the n observation in an arbitrary $y = \{y_1, \ldots, y_n\}$ is regarded as one point of the multivariate Gaussian distribution. The mean of this Gaussian distribution is often assumed to be zero. The covariance function (kernel function) $k(x, \acute{x})$ estimates the relationship between one observation to another one. The squared exponential is a popular choice to approximate function by the GPR model. Eq. (2) shows the calculation of the square of the exponential covariance function:

$$k(x, \acute{x}) = \sigma_f^2 \times exp\left(-\frac{(x-\acute{x})^2}{2l^2}\right) + \sigma_n^2 \delta(x, \acute{x}) \tag{2}$$

where σ_f^2 is the maximum allowable covariance. $k(x, \acute{x})$ is equal to this maximum if $x \approx \acute{x}$, which means $f(\acute{x})$ closely correlates $f(x)$. l is the length petameter, which defines the length of the kernel function. $\delta(x, \acute{x})$ is Kronecker delta function, which is defined by Eq. (3):

$$\delta_{ij} = \begin{cases} 1 \; if \; i = j \\ 0 \; if \; i \neq j \end{cases} \tag{3}$$

The ultimate objective of the learning process in the training dataset is to estimate the output value of y_* for a new input data. To reach this aim, three covariance matrices have to be defined as follows:

$$\begin{aligned} K &= \begin{bmatrix} k(x_1, x_1) & k(x_1, x_2) & \ldots & k(x_1, x_n) \\ k(x_2, x_1) & k(x_2, x_2) & \ldots & k(x_2, x_n) \\ \vdots & \vdots & \ddots & \vdots \\ k(x_n, x_1) & k(x_n, x_2) & \ldots & k(x_n, x_n) \end{bmatrix} \\ K_* &= [k(x_*, x_1) \quad k(x_*, x_2) \quad \ldots \quad k(x_*, x_n)] \\ K_{**} &= k(x_*, x_*) \end{aligned} \tag{4}$$

Based on the main assumption, we have:

$$\begin{bmatrix} y \\ y_* \end{bmatrix} \sim N\left(0, \begin{bmatrix} K & K_*^T \\ K_* & K_{**} \end{bmatrix}\right) \tag{5}$$

where T denotes matrix transposition.

Bayesian inference is used to determine the parameters of the GPR model, k and n, after estimating the hyperparameters of kernel function. The GPR model can estimate unknown data using the specified input data after training.

3.2. Evaluation metrics

In this study, the performance of the GPR model has been evaluated by various performance metrics such as RMSE (Root Mean Squared Error), MAD (Mean Absolute Deviation), MAE (Mean Absolute Error), R^2 (coefficient of determination), MAPE (Mean Absolute Percentage Error), and. These evaluation metrics are calculated as follows:

$$R^2 = \left[\frac{N\sum_{i=1}^{N} m_i p_i - \sum_{i=1}^{N} m_i \sum_{i=1}^{N} p_i}{\sqrt{N\sum_{i=1}^{N} m_i{}^2 - \left(\sum_{i=1}^{N} m_i\right)^2}\sqrt{N\sum_{i=1}^{N} p_i{}^2 - \left(\sum_{i=1}^{N} p_i\right)^2}}\right]^2 \tag{6}$$

$$RMSE = \sqrt{\frac{1}{N}\sum_{i=1}^{N}(m_i - p_i)^2} \tag{7}$$

$$MAE = \frac{1}{N}\sum_{i=1}^{N}|m_i - p_i| \tag{8}$$

$$MAPE = \frac{1}{N}\sum_{i=1}^{N}\left|\frac{m_i - p_i}{m_i}\right| * 100 \tag{9}$$

$$RRSE = \sqrt{\frac{\sum_{i=1}^{N}(m_i - p_i)^2}{\sum_{i=1}^{N}\left(m_i - \frac{1}{N}\sum_{i=1}^{N} m_i\right)^2}} \tag{10}$$

$$RAE = \frac{\sum_{i=1}^{N}|m_i - p_i|}{\sum_{i=1}^{N}\left|m_i - \frac{1}{N}\sum_{i=1}^{N} m_i\right|} \tag{11}$$

where N is the number of observations for the evaluation of the desired model, p_i is the predicted value and m_i is the measured value for the i^{th} data point.

4. Modeling UCS and E using the Gaussian process regression (GPR)

A MATLAB program was developed to train and test the GPR models. 70% and 30% of the data have been randomly selected for the training and the testing set, respectively, to model the UCS and the E of the samples. Linear basis function and squared exponential kernel function were chosen by trial and error to develop the final model. The input variables of the GPR model were IMOT percentage, HL percentage, MC, and CT, while the output variables of the GPR model were UCS and E. The measured and predicted values of the UCS and E are reported in the dataset in the Appendix.

The evaluation metrics for the GPR model are presented for the training and testing sets as well as the overall in Table 5.

Table 5
Performance metrics for the GPR model.

Evaluation Metrics	Training	Testing	Total
	UCS		
R^2	0.9866	0.9731	0.9825
RMSE	0.1625	0.2359	0.1875
RAE	0.0976	0.1484	0.1127
RRSE	0.0135	0.0282	0.0179
MAE	0.1116	0.1689	0.1287
MAPE	4.8823	7.5752	5.6865
	Young's Modulus (E)		
R^2	0.9788	0.9252	0.9633
RMSE	15.408	27.605	19.868
RAE	0.1296	0.2342	0.1600
RRSE	0.0213	0.0779	0.0368
MAE	11.519	20.077	14.083
MAPE	10.091	14.060	11.280

The performance of the GPR model for estimating the UCS and the E of the clay soils stabilized with IOMT and HL are shown in Fig. 2 and 3, respectively. As can be observed, the values of R^2 for estimating the UCS are 0.9866 and 0.9731 for the training set and the testing set, respectively. The RMSE for estimating the UCS are 0.1625 and 0.2359 for the training set and the testing set, respectively. Moreover, the values of the R^2 for estimating the E are 0.9788 and 0.9252 for the training set and the testing set, respectively. The RMSE for estimating the E are 15.408 and 27.605 for the training set and the testing set, respectively.

The comparison of the measured and predicted UCS and E by the GPR model is depicted in Fig. 4 and 5, respectively. The absolute relative error (ARE) is also depicted for each data in these figures. As shown in Fig. 6 and 7, only three data points have an ARE more than 20% for the prediction of UCS, while 25 data points have an ARE more than 20% for the prediction of E by the GPR model.

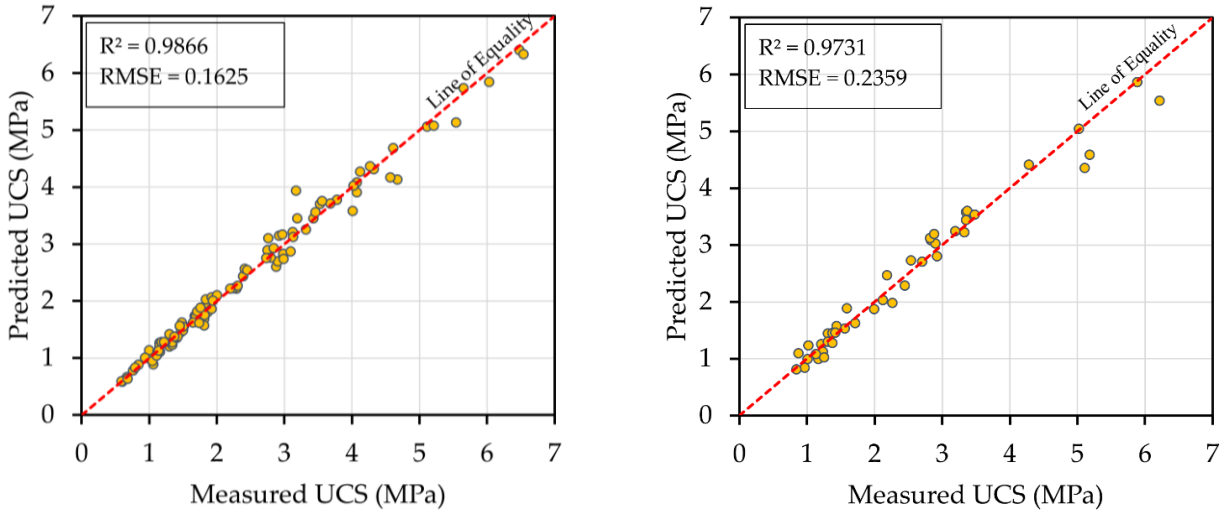

(a) (b)

Fig. 4. The performance of the GPR model for predicting UCS: (a) The training set, (b) The testing set.

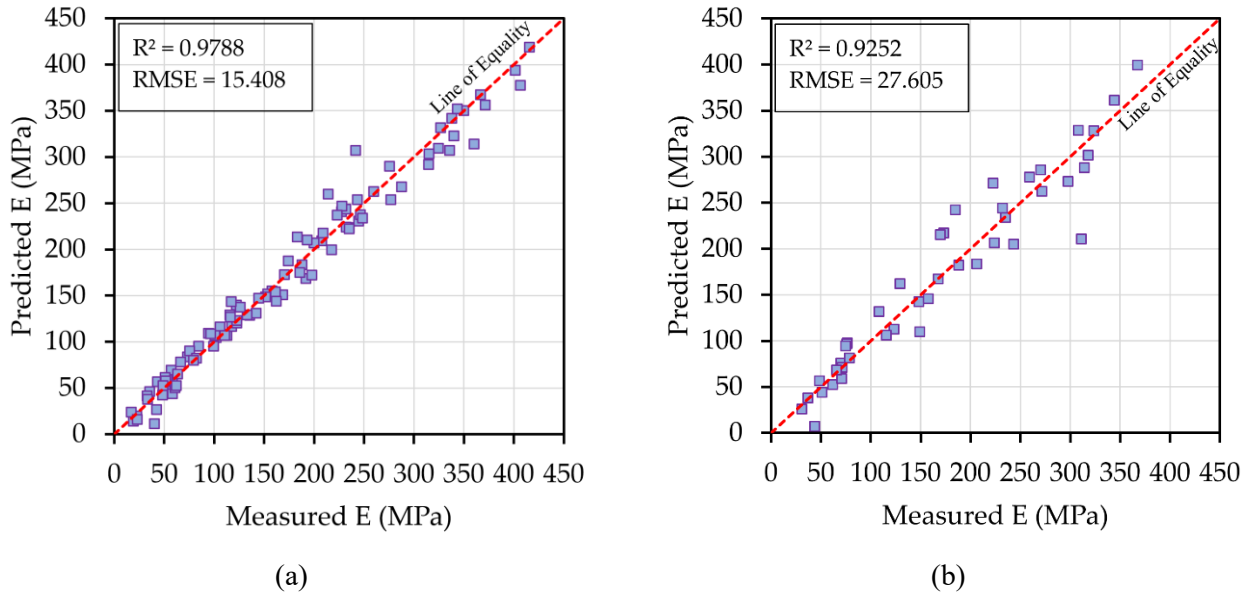

Fig. 5. The performance of the GPR model for predicting E: (a) The training set, (b) The testing set.

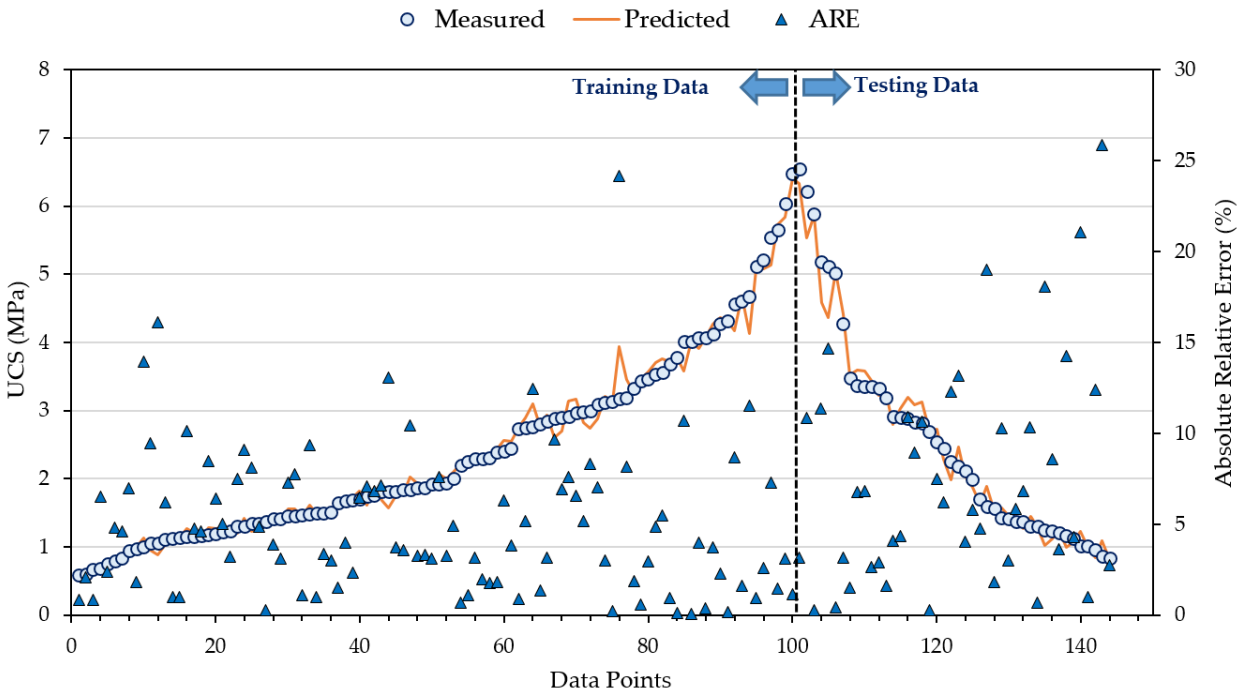

Fig. 6. Comparison of measured and predicted UCS using the GPR model.

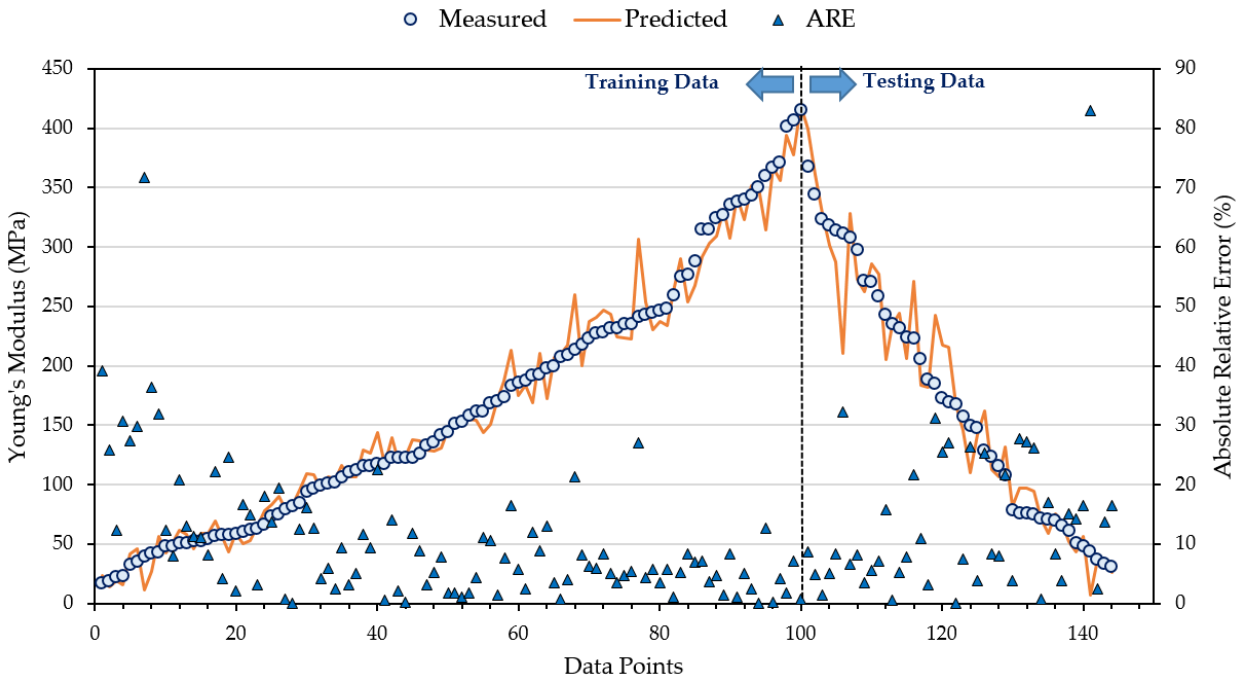

Fig. 7. Comparison of measured and predicted the Young's modulus using the GPR model.

5. Performance comparison of GPR with ANN

The performance of the GPR model to estimate the UCS and E of the stabilized clay soil was compared with ANN to evaluate the capabilities of the GPR method in this case. In this regard, a multi-layer perception (MLP) with the backpropagation algorithm was used. The optimal architecture of ANN was determined by trial and error. To this end, a MATLAB program was utilized to obtain the number of neurons in the hidden layers. The number of neurons was selected between 2 to 20. The transfer function of the hidden layer and output layer were selected as tangent sigmoid and linear, respectively. 70% of data where used as the training and validation (60% for training and 10% for validating), while 30% of data were used for testing. Similar to GPR model, four input parameters including IOMT, HL, MC, and CT were considered as input variables in building ANN model. According to the results, the ANN with 12 and 17 neurons in the hidden layer has optimal accuracy in the estimation of the UCS and the E, respectively. Therefore, the architecture of the ANN was selected as 4-12-1 and 4-17-1 for estimating the UCS and the E, respectively. Table 6 demonstrates the performance of the GPR and the ANN models in terms of R^2 and RMSE. As can be seen, the values R^2 and RMSE of the GPR model to estimate the UCS for training, testing, and total data are better than the ANN model. Moreover, the values R^2 and RMSE of the GPR model to predict the E for the training set and the total data is higher than the ANN model. The ANN model only performs better to predict the E in the testing set. In total, it is found that the GPR model is more efficient to estimate the UCS and the E of the clay soil stabilized with IOMT.

Table 6
The performance comparison of the GPR model with the ANN model.

	Training	Testing	Total	Training	Testing	Total
Model	UCS (R^2)			UCS (RMSE)		
ANN	0.9726	0.9605	0.9692	0.2372	0.2665	0.2463
GPR	0.9866	0.9731	0.9825	0.1625	0.2359	0.1875
Model	Young's Modulus (R^2)			Young's Modulus (RMSE)		
ANN	0.9678	0.9576	0.9624	17.823	26.201	20.6951
GPR	0.9788	0.9252	0.9633	15.408	27.605	19.868

6. Sensitivity analysis

It is essential to carry out different analyses on the proposed model to validate and test robustness of the model for unknown data. Sensitivity analysis determines the effects of the input variables on the output of the model. The sensitivity analysis method used in this study was adopted from Gandomi et al. [42] and Javed et al. [43]. This sensitivity analysis method determines the contribution of the input variables to the predicted output. To this end, the sensitivity percentage (*SP*) of the output for any input variable is calculated by Eq. (12) and (13):

$$I_i = f_{max}(p_i) - f_{min}(p_i) \tag{12}$$

$$SP_i = \frac{I_i}{\sum_j^n I_j} \times 100 \tag{13}$$

where $f_{min}(p_i)$ and $f_{max}(p_i)$ are the minimum and maximum value of the outputs of the predictive model based on the i^{th} input variable, where the rest of input variables are equal to their average value. The sensitivity percentage of 100 demonstrates the highest contribution, while $SP = 0$ shows the lowest.

The sensitivity analysis of the GPR model for the predicted outputs is shown in Fig. 8. As it can be seen in Fig. 8(a), the moisture content (MC), curing time (CT), hydrated lime (HL) percentage, and iron ore mine tailings (IOMC) percentage have the highest contribution to the UCS of the stabilized clay samples, respectively. Fig. 8(b) demonstrates that MC, HL, IOMT, and CT have the highest effect on the Young's Modulus of the stabilized clay samples, respectively.

7. Parametric analysis

The parametric analysis (Fig. 9 to 14) was performed to examine the influence of an input on the E and the UCS of samples. To perform this analysis, the value of the desired variable was changed and other variables were kept constant. Constant values are shown on each Figure. These Figures show that the general trend of changes in UCS and E is almost the same.

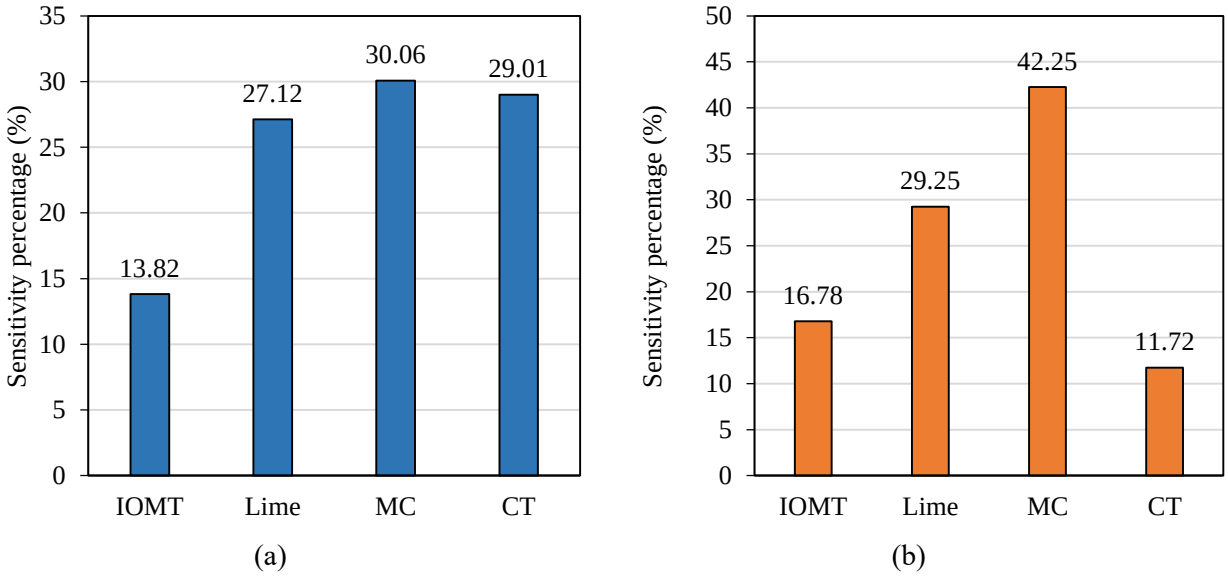

Fig. 8. Sensitivity analysis of the GPR model for (a) UCS, (b) Young's Modulus (E).

Fig. 9 and 12 show that by increasing the HL content up to about 4%, the UCS and E increase, and by increasing the percentage of HL to more than this amount, the UCS and E decrease. Past researches show that the UCS of soils stabilized with HL increases as long as there is silica and alumina in the soil to react with HL, and after these two are exhausted, due to the lack of reaction between soil and HL, the UCS decreases [12,44–46]. Fig. 10 and 13 show that the UCS and the E decrease with increasing moisture content. In fact, like the compressive strength of concrete, with the increase in moisture content, the ratio of water to cement increases, which causes the strength of stabilized materials to decrease. Also, as expected, according to Fig. 11 and 14, the UCS and the E increase with increasing curing time. In addition, as shown in Fig. 9 to 14, with the increase in IOMT percentage, the UCS and the E decrease. The reason for this is the decrease in the amount of alumina and silica in the soil due to replacing of some fraction of the soil with IOMT.

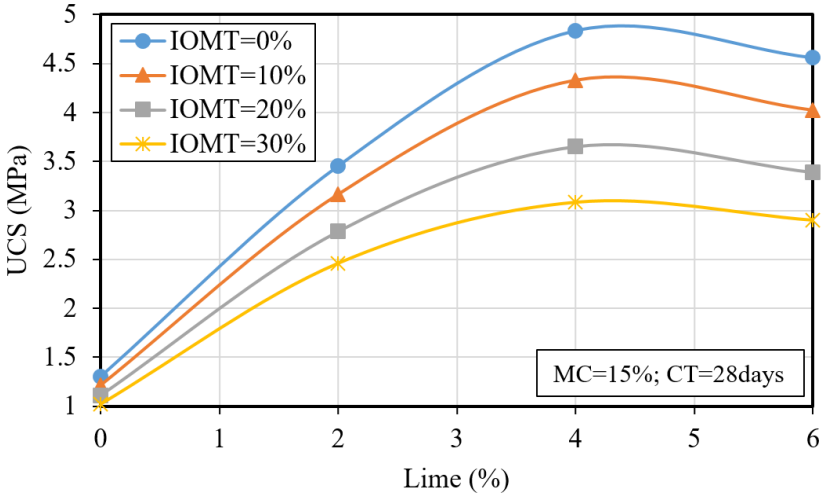

Fig. 9. Effect of HL content on the UCS based on the GPR model.

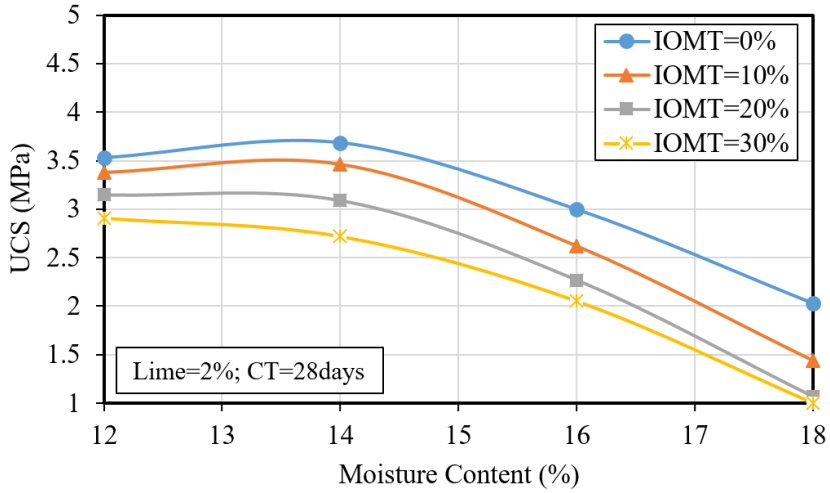

Fig. 10. Effect of moisture content on the UCS based on the GPR model.

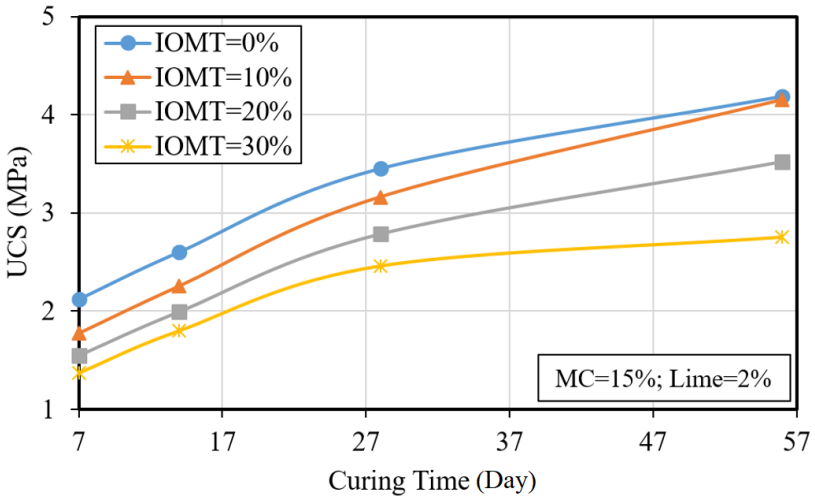

Fig. 11. Effect of curing time on the UCS based on the GPR model.

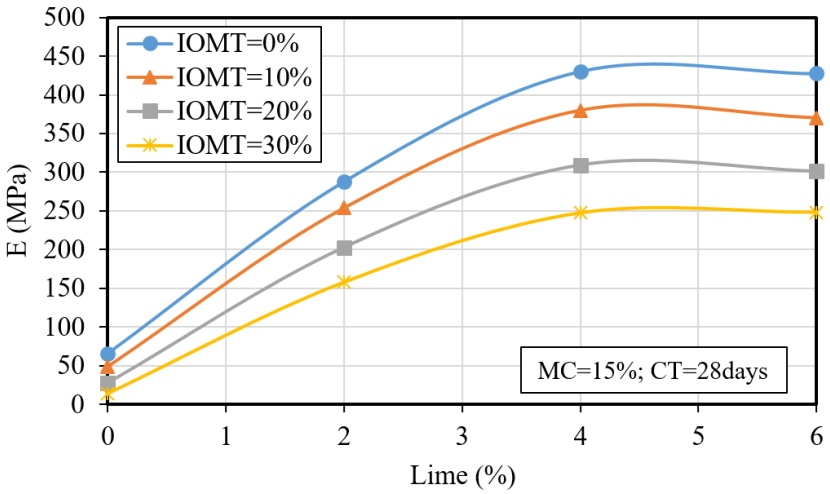

Fig. 12. Effect of HL content on the Young's modulus based on the GPR model.

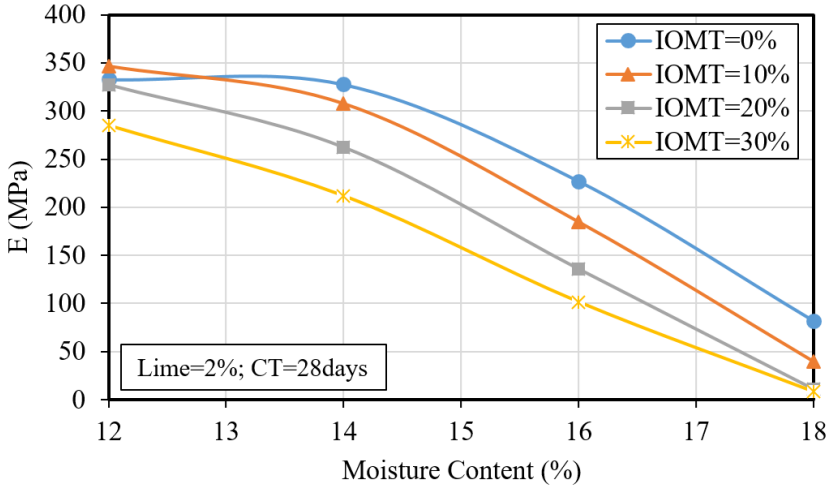

Fig. 13. Effect of moisture content on the Young's modulus based on the GPR model.

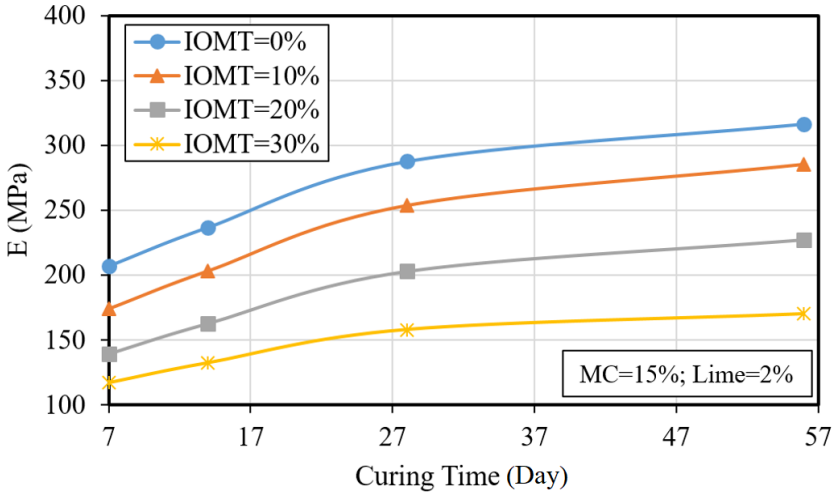

Fig. 14. Effect of curing time on the Young's modulus based on the GPR model.

8. Conclusion

In this study, gaussian process regression (GPR) was used to estimate the UCS and the Young's modulus (E) of the clay soils stabilized with hydrated lime and IOMT. To this end, a GPR model was developed based on four input variables including HL percentage, IOMT percentage, MC, and CT. The R^2 and RMSE values for the GPR model to estimate the UCS were 0.9866 and 0.1625 for the training set, 0.9731 and 0.2359 for the testing set, and 0.9825 and 0.1875 for the overall data, respectively. In addition, the R^2 and RMSE values of the GPR model to estimate the E were 0.9788 and 15.408 for the training set, 0.9252 and 27.605 for the testing set, and 0.9633 and 19.868 for the overall data, respectively. The sensitivity analysis demonstrated that the MC, CT, HL, and IOMT have the highest contribution to the UCS of the stabilized lean clay, respectively. Also, MC, HL, IOMT percentage, and CT have the highest effect on the E of the stabilized lean clay, respectively. The parametric study shows that with increasing the HL content

up to a certain value, the strength parameters of the soil stabilized with HL and IOMT increase, and then the strength parameters decrease with the increase of the percentage of HL. Also, the strength parameters of soil stabilized with HL and IOMT increase with increasing curing time and decrease with increasing moisture content and IOMT percentage.

Funding

This research received no external funding.

Conflicts of interest

The authors declare no conflict of interest.

Authors contribution statement

ARG, SSN: Conceptualization; ARG, SSN: Formal analysis; ARG, SSN: Investigation; ARG, SSN: Methodology; ARG: Project administration; ARG: Software; ARG, SSN: Visualization; ARG, SSN: Roles/Writing – original draft; ARG, SSN: Writing – review & editing.

Appendix

The database used in this research is given below.

No.	IOMT (%)	HL (%)	MC (%)	CT (days)	Measured UCS (MPa)	Predicted UCS (MPa)	Measured E (MPa)	Predicted E (MPa)
1	20	0	12.33	56	1.67	1.74	105.94	115.94
2	10	4	18.3711	56	3.53	3.70	157.84	155.07
3	0	6	18.2	56	3.17	3.93	243.46	254.04
4	10	2	15.7	56	3.78	3.78	227.28	240.81
5	20	6	14.85	28	3.43	3.45	324.4	309.25
6	30	2	14.1	7	1.45	1.56	153.41	151.86
7	30	0	11.88	7	0.98	1.00	58.33	59.54
8	30	0	13.2	56	1.47	1.45	73.41	83.52
9	10	0	14.7	28	1.15	1.27	43.03	56.75
10	20	4	17.49	28	2.3	2.25	135.53	128.48
11	30	0	11.88	56	1.69	1.73	102.04	104.60
12	20	4	15.9	7	1.5	1.49	151.33	148.51
13	30	4	16.28	28	2.88	2.60	191.84	168.72
14	10	6	15.813	28	3.46	3.56	340	322.99
15	20	4	14.31	56	6.03	5.84	366.63	367.17
16	10	4	15.0309	56	6.48	6.40	401.23	393.93
17	20	4	14.31	28	4.07	3.91	371.38	356.08
18	10	6	19.327	28	1.87	1.93	100.87	106.91
19	30	2	15.51	56	2.39	2.43	122.98	137.47
20	10	6	15.813	7	1.81	1.68	174.15	187.38

No.	IOMT (%)	HL (%)	MC (%)	CT (days)	Measured UCS (MPa)	Predicted UCS (MPa)	Measured E (MPa)	Predicted E (MPa)
21	0	6	16.38	28	3.68	3.71	350	350.10
22	30	2	14.1	56	3.12	3.21	235	223.87
23	20	2	14.9	28	2.98	2.83	207.7	209.35
24	10	4	18.3711	7	1.16	1.11	58.24	55.83
25	0	2	16.2	56	3.56	3.75	277	253.78
26	0	2	16.2	7	1.84	1.77	168.62	150.81
27	0	2	14.58	56	4.12	4.27	326.85	331.57
28	30	6	14.13	7	1.65	1.62	188.01	183.34
29	30	2	12.69	7	1.87	1.81	217.54	199.81
30	30	4	14.8	28	2.92	3.14	213.99	259.78
31	0	0	16.9224	56	1.3	1.20	52.48	46.52
32	30	6	14.13	56	5.11	5.06	314.55	291.80
33	10	0	16.17	28	1.06	0.89	40.03	11.34
34	30	2	12.69	28	3.09	2.87	287.72	267.58
35	30	6	17.27	28	2.29	2.22	144.65	147.35
36	0	2	16.2	28	2.75	2.89	183.4	213.51
37	0	6	20.02	28	2.25	2.23	112.71	106.96
38	30	6	17.27	7	1	1.14	56.79	69.44
39	0	6	20.02	7	1.15	1.21	54.75	59.24
40	30	4	14.8	7	1.51	1.56	185.8	175.04
41	30	4	13.32	7	1.92	1.86	231.81	243.44
42	0	2	14.58	28	4.01	3.58	335.51	307.24
43	20	0	15.07	7	0.67	0.66	22.41	19.66
44	20	2	13.41	28	2.97	3.16	275.45	289.89
45	20	2	13.41	56	4.07	4.08	359.94	314.09
46	20	4	17.49	56	3.32	3.26	161.39	154.30
47	20	2	16.39	28	1.84	2.03	94.23	109.38
48	30	2	14.1	28	2.9	2.70	200	206.96
49	20	2	14.9	7	1.81	1.57	162.09	144.12
50	30	6	17.27	56	2.84	2.93	170.31	172.72
51	10	0	16.17	56	1.34	1.23	58.24	43.91
52	0	0	13.8456	56	1.48	1.62	96.62	108.83
53	10	4	15.0309	7	1.92	2.07	228.03	247.04
54	10	6	17.57	28	2.41	2.56	193.21	210.31
55	0	6	18.2	7	1.5	1.55	141.87	130.84
56	10	2	15.7	7	1.45	1.56	122.34	139.62
57	30	0	13.2	28	1.2	1.28	53.05	58.94
58	0	2	17.82	28	2	2.10	84.57	95.10
59	0	0	15.384	7	0.84	0.88	35.45	46.01
60	10	0	13.23	56	1.82	1.75	117.39	116.74
61	10	2	17.27	28	1.71	1.82	75.51	90.25
62	10	0	14.7	56	1.74	1.62	99.46	95.33

No.	IOMT (%)	HL (%)	MC (%)	CT (days)	Measured UCS (MPa)	Predicted UCS (MPa)	Measured E (MPa)	Predicted E (MPa)
63	0	2	17.82	7	1.34	1.27	63.36	65.40
64	0	6	16.38	7	1.94	2.00	209.13	217.66
65	30	0	14.52	28	1.12	1.11	42.26	26.90
66	30	2	15.51	28	2.31	2.27	133.11	129.00
67	20	0	13.7	28	1.18	1.28	50.96	61.53
68	30	4	16.28	7	1.24	1.28	110.49	106.94
69	10	0	16.17	7	0.6	0.59	19.14	14.18
70	0	4	17.2	56	5.54	5.14	315.18	303.43
71	30	0	13.2	7	0.76	0.78	32.7	41.69
72	0	4	18.92	56	4.67	4.13	197.83	172.12
73	30	0	14.52	7	0.59	0.60	17.19	23.91
74	0	0	13.8456	28	1.3	1.42	66.25	78.24
75	30	6	15.7	7	1.41	1.36	122.82	120.27
76	0	6	20.02	56	3.13	3.12	126.14	137.34
77	0	2	17.82	56	2.76	3.10	117.26	143.62
78	0	4	18.92	28	2.8	2.76	122.83	123.16
79	0	0	13.8456	7	0.94	1.01	51.15	57.84
80	20	2	16.39	56	2.45	2.54	115.56	129.07
81	20	0	12.33	28	1.42	1.38	82.07	82.14
82	10	0	13.23	7	1.05	0.95	60.59	50.47
83	30	4	13.32	28	3.19	3.45	337.96	341.90
84	20	4	14.31	7	1.76	1.88	223.2	237.25
85	20	6	14.85	56	5.65	5.73	241.62	307.01
86	30	4	13.32	56	5.21	5.07	343.43	351.85
87	10	2	17.27	56	2.73	2.75	116.02	126.94
88	0	0	16.9224	7	0.68	0.64	23.06	15.96
89	20	4	15.9	56	4.61	4.68	259.71	262.40
90	10	4	15.0309	28	4.32	4.31	406.57	377.56
91	30	6	15.7	56	4.02	4.02	244.79	230.75
92	20	6	18.15	7	1.11	1.04	61.96	52.71
93	10	6	17.57	56	4.57	4.17	246.33	237.68
94	10	0	13.23	28	1.37	1.37	79.13	79.78
95	0	4	15.48	56	6.54	6.33	415.62	418.93
96	0	6	18.2	28	2.99	2.74	232.16	224.19
97	20	6	16.5	56	4.27	4.37	248.32	233.82
98	20	0	15.07	56	1.22	1.28	48.62	52.49
99	0	2	14.58	7	2.2	2.22	235.08	222.38
100	30	0	14.52	56	1.14	1.13	48.43	42.43
101	20	0	13.7	7	0.79	0.83	33.22	37.78
102	20	6	14.85	7	1.71	1.63	206.2	183.72
103	30	4	14.8	56	5.11	4.36	297.61	273.00
104	30	2	15.51	7	1.21	1.25	76.39	97.58

No.	IOMT (%)	HL (%)	MC (%)	CT (days)	Measured UCS (MPa)	Predicted UCS (MPa)	Measured E (MPa)	Predicted E (MPa)
105	20	6	18.15	56	2.83	3.08	129.16	161.91
106	10	4	16.701	56	5.02	5.04	258.98	277.57
107	20	0	12.33	7	1.01	1.00	61.64	52.38
108	10	6	19.327	7	1.16	0.99	51.18	43.93
109	10	6	19.327	56	2.9	3.03	148.25	142.53
110	20	2	14.9	56	3.35	3.58	235.22	233.97
111	10	2	14.13	7	2.26	1.98	311.07	210.70
112	10	2	15.7	28	2.92	2.80	223.79	206.38
113	20	6	16.5	28	2.54	2.73	173.26	217.37
114	10	4	18.3711	28	2.44	2.29	123.28	112.88
115	0	4	15.48	28	5.18	4.59	367.62	399.39
116	20	6	18.15	28	2.12	2.03	108.23	131.71
117	0	4	15.48	7	2.18	2.47	222.73	271.05
118	30	2	12.69	56	3.37	3.60	270.35	285.54
119	20	2	16.39	7	1.23	1.12	69.92	75.75
120	30	6	14.13	28	2.82	3.12	314.08	287.89
121	10	2	14.13	28	3.35	3.44	318.01	301.71
122	0	0	15.384	28	1.02	1.23	48.63	56.69
123	30	0	11.88	28	1.31	1.45	78.57	81.54
124	10	2	17.27	7	1.25	1.02	71.08	59.00
125	0	6	16.38	56	6.21	5.54	344.26	361.28
126	20	0	15.07	28	0.87	1.10	31.02	25.88
127	10	4	16.701	28	3.19	3.24	232.16	244.28
128	20	6	16.5	7	1.31	1.30	149.23	109.92
129	10	4	16.701	7	1.56	1.53	157.72	145.97
130	0	4	18.92	7	1.37	1.45	71.49	70.97
131	30	6	15.7	28	2.7	2.71	169.57	215.39
132	0	0	16.9224	28	0.96	0.84	43.86	7.47
133	20	0	13.7	56	1.43	1.58	76.17	96.86
134	30	4	16.28	56	3.32	3.22	188.25	182.39
135	10	6	15.813	56	5.88	5.86	323.73	328.27
136	20	4	15.9	28	2.88	3.19	184.77	242.56
137	0	0	15.384	56	1.42	1.46	74.86	94.51
138	20	4	17.49	7	1.13	1.08	65.79	68.30
139	10	2	14.13	56	4.28	4.42	308.11	328.73
140	0	4	17.2	7	1.59	1.89	167.37	167.36
141	10	6	17.57	7	1.37	1.28	115.69	106.32
142	0	4	17.2	28	3.48	3.53	271.59	262.24
143	20	2	13.41	7	1.99	1.87	243.4	205.08
144	10	0	14.7	7	0.84	0.82	36.93	37.87

References

[1] Gurbuz A. Marble powder to stabilise clayey soils in sub-bases for road construction. Road Mater Pavement Des 2015;16:481–92. https://doi.org/10.1080/14680629.2015.1020845.

[2] Firoozi AA, Guney Olgun C, Firoozi AA, Baghini MS. Fundamentals of soil stabilization. Int J Geo-Engineering 2017;8:1–16. https://doi.org/10.1186/s40703-017-0064-9.

[3] Mukesh AP, Patel HS. A review on the effects of stabilizing agents for stabilization of weak soil. Civ Environ Res 2012;2:1–7.

[4] Afrin H. A Review on Different Types Soil Stabilization Techniques. Int J Transp Eng Technol 2017;3:19. https://doi.org/10.11648/j.ijtet.20170302.12.

[5] Keskin İ, Kahraman S. Stabilization of swelling soil by lime, fly ash, and calcium carbide residue. Arab J Geosci 2022;15:1009. https://doi.org/10.1007/s12517-022-10291-3.

[6] Kumar GS, Shankar S. Strength and Durability Characteristics of Lime Fly Ash-Stabilized Recycled Concrete Aggregate for Use in Low-Volume Rural Roads. Indian Geotech J 2022:1–15. https://doi.org/10.1007/s40098-022-00659-3.

[7] Olinic T, Olinic E. The Effect of Quicklime Stabilization on Soil Properties. Agric Agric Sci Procedia 2016;10:444–51. https://doi.org/10.1016/j.aaspro.2016.09.013.

[8] Dhar S, Hussain M. The strength and microstructural behavior of lime stabilized subgrade soil in road construction. Int J Geotech Eng 2021;15:471–83. https://doi.org/10.1080/19386362.2019.1598623.

[9] Jahandari S, Saberian M, Zivari F, Li J, Ghasemi M, Vali R. Experimental study of the effects of curing time on geotechnical properties of stabilized clay with lime and geogrid. Int J Geotech Eng 2019;13:172–83. https://doi.org/10.1080/19386362.2017.1329259.

[10] Sridevi G, Sahoo S, Sen S. Stabilization of Expansive Soil with Red Mud and Lime. Lect. Notes Civ. Eng., vol. 14, Springer; 2019, p. 259–68. https://doi.org/10.1007/978-981-13-0559-7_29.

[11] Zilaei M, Ghanizadeh AR. Strength and Durability of Iron Ore Tailing Materials Stabilized using Portland Cement as Base Materials: A Case Study Of Golgohar Mine. J Transp Infrastruct Eng 2021;7:101–22.

[12] Ghanizadeh AR, Zolfaghari M, Abbaslou H. Mechanical Properties and durability of clayey subgrade stabilized with iron ore mine tailing and hydrated lime. J Transp Infrastruct Eng 2020;6:69–88. https://doi.org/10.22075/jtie.2020.18494.1410.

[13] Etim RK, Eberemu AO, Osinubi KJ. Stabilization of black cotton soil with lime and iron ore tailings admixture. Transp Geotech 2017;10:85–95. https://doi.org/10.1016/j.trgeo.2017.01.002.

[14] Bastos LA de C, Silva GC, Mendes JC, Peixoto RAF. Using Iron Ore Tailings from Tailing Dams as Road Material. J Mater Civ Eng 2016;28:4016102. https://doi.org/10.1061/(asce)mt.1943-5533.0001613.

[15] Li H Bin. Experimental research on performance of road base with cement stabilized iron tailings sand. Appl. Mech. Mater., vol. 513–517, Trans Tech Publ; 2014, p. 60–4. https://doi.org/10.4028/www.scientific.net/AMM.513-517.60.

[16] Osinubi KJ, Yohanna P, Eberemu AO. Cement modification of tropical black clay using iron ore tailings as admixture. Transp Geotech 2015;5:35–49. https://doi.org/10.1016/j.trgeo.2015.10.001.

[17] Xu S. Research on Application of Iron Tailings on Road Base. Adv Mater Res 2013;743:54–7. https://doi.org/10.4028/www.scientific.net/AMR.743.54.

[18] Shishegaran A, Varaee H, Rabczuk T, Shishegaran G. High correlated variables creator machine: Prediction of the compressive strength of concrete. Comput Struct 2021;247:106479. https://doi.org/10.1016/j.compstruc.2021.106479.

[19] Hoang ND, Tran VD. Deep Neural Network Regression with Advanced Training Algorithms for Estimating the Compressive Strength of Manufactured-Sand Concrete. J Soft Comput Civ Eng 2023;7:114–34. https://doi.org/10.22115/SCCE.2022.349837.1485.

[20] Ghanizadeh AR, Ghanizadeh A, Asteris PG, Fakharian P, Armaghani DJ. Developing bearing capacity model for geogrid-reinforced stone columns improved soft clay utilizing MARS-EBS hybrid method. Transp Geotech 2023;38:100906. https://doi.org/10.1016/j.trgeo.2022.100906.

[21] Ghanizadeh AR, Heidarabadizadeh N, Heravi F. Gaussian process regression (Gpr) for auto-estimation of resilient modulus of stabilized base materials. J Soft Comput Civ Eng 2021;5:80–94. https://doi.org/10.22115/SCCE.2021.269187.1273.

[22] Ghanizadeh AR, Bayat M, Tavana Amlashi, A Rahrovan M. Prediction of Unconfined Compressive Strength of Clay Subgrade Soil Stabilized With Portland Cement and Lime Using Group Method of Data Handling (GMDH). J Transp Infrastruct Eng 2019;5:77–96.

[23] Ghanizadeh AR, Delaram A, Fakharian P, Armaghani DJ. Developing Predictive Models of Collapse Settlement and Coefficient of Stress Release of Sandy-Gravel Soil via Evolutionary Polynomial Regression. Appl Sci 2022;12:9986. https://doi.org/10.3390/app12199986.

[24] Ghanizadeh AR, Heidarabadizadeh N, Bayat M, Khalifeh V. Modeling of unconfined compressive strength and Young's modulus of lime and cement stabilized clayey subgrade soil using Evolutionary Polynomial Regression (EPR). Int J Min Geo-Engineering 2022;56:257–69. https://doi.org/10.22059/IJMGE.2022.306688.594858.

[25] Shishegaran A, Karami B, Safari Danalou E, Varaee H, Rabczuk T. Computational predictions for predicting the performance of steel 1 panel shear wall under explosive loads. Eng Comput (Swansea, Wales) 2021;ahead-of-p. https://doi.org/10.1108/EC-09-2020-0492.

[26] Momeni E, Dowlatshahi MB, Omidinasab F, Maizir H, Armaghani DJ. Gaussian Process Regression Technique to Estimate the Pile Bearing Capacity. Arab J Sci Eng 2020;45:8255–67. https://doi.org/10.1007/s13369-020-04683-4.

[27] Indraratna B, Armaghani DJ, Correia AG, Hunt H, Ngo T. Prediction of resilient modulus of ballast under cyclic loading using machine learning techniques. Transp Geotech 2022:100895.

[28] Sathyapriya S, Arumairaj PD, Ranjini D. Prediction of Unconfined Compressive Strength of a Stabilised Expansive Clay Soil using ANN and Regression Analysis (SPSS). Asian J Res Soc Sci Humanit 2017;7:109. https://doi.org/10.5958/2249-7315.2017.00075.2.

[29] Chore HS, Magar RB. Prediction of unconfined compressive and brazilian tensile strength of fiber reinforced cement stabilized fly ash mixes using multiple linear regression and artificial neural network. Adv Comput Des 2017;2:225–40. https://doi.org/10.12989/acd.2017.2.3.225.

[30] Sihag P, Suthar M, Mohanty S. Estimation of UCS-FT of Dispersive Soil Stabilized with Fly Ash, Cement Clinker and GGBS by Artificial Intelligence. Iran J Sci Technol - Trans Civ Eng 2021;45:901–12. https://doi.org/10.1007/s40996-019-00329-0.

[31] Tabarsa A, Latifi N, Osouli A, Bagheri Y. Unconfined compressive strength prediction of soils stabilized using artificial neural networks and support vector machines. Front Struct Civ Eng 2021;15:520–36. https://doi.org/10.1007/s11709-021-0689-9.

[32] Do H-D, Pham V-N, Nguyen H-H, Huynh P-N, Han J. Prediction of Unconfined Compressive Strength and Flexural Strength of Cement-Stabilized Sandy Soils: A Case Study in Vietnam. Geotech Geol Eng 2021;39:4947–62. https://doi.org/10.1007/s10706-021-01805-z.

[33] Pham BT, Nguyen MD, Nguyen-Thoi T, Ho LS, Koopialipoor M, Kim Quoc N, et al. A novel approach for classification of soils based on laboratory tests using Adaboost, Tree and ANN modeling. Transp Geotech 2021;27:100508. https://doi.org/10.1016/j.trgeo.2020.100508.

[34] Tran VQ. Hybrid gradient boosting with meta-heuristic algorithms prediction of unconfined compressive strength of stabilized soil based on initial soil properties, mix design and effective compaction. J Clean Prod 2022;355:131683. https://doi.org/10.1016/j.jclepro.2022.131683.

[35] Armaghani DJ, Mirzaei F, Shariati M, Trung NT, Shariati M, Trnavac D. Hybrid ann-based techniques in predicting cohesion of sandy-soil combined with fiber. Geomech Eng 2020;20:191–205. https://doi.org/10.12989/gae.2020.20.3.191.

[36] Momeni E, Yarivand A, Dowlatshahi MB, Armaghani DJ. An Efficient Optimal Neural Network Based on Gravitational Search Algorithm in Predicting the Deformation of Geogrid-Reinforced Soil Structures. Transp Geotech 2021;26:100446.

[37] Momeni E, He B, Abdi Y, Armaghani DJ. Novel Hybrid XGBoost Model to Forecast Soil Shear Strength Based on Some Soil Index Tests. C Model Eng Sci 2022.

[38] Ahmad M, Keawsawasvong S, Bin Ibrahim MR, Waseem M, Kashyzadeh KR, Sabri MMS. Novel Approach to Predicting Soil Permeability Coefficient Using Gaussian Process Regression. Sustain 2022;14:8781. https://doi.org/10.3390/su14148781.

[39] Samui P, Jagan J. Determination of effective stress parameter of unsaturated soils: A Gaussian process regression approach. Front Struct Civ Eng 2013;7:133–6. https://doi.org/10.1007/s11709-013-0202-1.

[40] Schulz E, Speekenbrink M, Krause A. A tutorial on Gaussian process regression: Modelling, exploring, and exploiting functions. J Math Psychol 2018;85:1–16. https://doi.org/10.1016/j.jmp.2018.03.001.

[41] Liu M, Huang C, Wang L, Zhang Y, Luo X. Short-term soil moisture forecasting via gaussian process regression with sample selection. Water (Switzerland) 2020;12:1–17. https://doi.org/10.3390/w12113085.

[42] Gandomi AH, Yun GJ, Alavi AH. An evolutionary approach for modeling of shear strength of RC deep beams. Mater Struct 2013;46:2109–19. https://doi.org/10.1617/s11527-013-0039-z.

[43] Javed MF, Amin MN, Shah MI, Khan K, Iftikhar B, Farooq F, et al. Applications of gene expression programming and regression techniques for estimating compressive strength of bagasse ash based concrete. Crystals 2020;10:1–17. https://doi.org/10.3390/cryst10090737.

[44] Asgari MR, Baghebanzadeh Dezfuli A, Bayat M. Experimental study on stabilization of a low plasticity clayey soil with cement/lime. Arab J Geosci 2015;8:1439–52. https://doi.org/10.1007/s12517-013-1173-1.

[45] Goodarzi AR. Effect of curing temperature and SiO2-nanoparticles on the engineering properties of lime treated expansive soil. Modares Civ Eng J 2017;17:132–44.

[46] Khemissa M, Mahamedi A. Cement and lime mixture stabilization of an expansive overconsolidated clay. Appl Clay Sci 2014;95:104–10. https://doi.org/10.1016/j.clay.2014.03.017.